Surface protrusion induced by inter-diffusion on Cu-Sn micro-pillars

Chen, Yang; Dai, Wenjie; Liu, Yingxia; Chen, Chih ; Tu, K.N.; Chen, Guang

Published in:
Materials & Design

Published: 01/12/2022

Published version (DOI):
10.1016/j.matdes.2022.111318

Publication details:
Chen, Y., Dai, W., Liu, Y., Chen, C., Tu, K. N., & Chen, G. (2022). Surface protrusion induced by inter-diffusion on Cu-Sn micro-pillars. *Materials & Design*, *224*, Article 111318. https://doi.org/10.1016/j.matdes.2022.111318

Materials & Design 224 (2022) 111318

Contents lists available at ScienceDirect

Materials & Design

journal homepage: www.elsevier.com/locate/matdes

Surface protrusion induced by inter-diffusion on Cu-Sn micro-pillars

Yang Chen [a,b,1], Wenjie Dai [b,1], Yingxia Liu [a], Chih Chen [c], K.N. Tu [a,c,*], Guang Chen [b,*]

[a] Dept. of Materials Science and Engineering, Uni. of California, Los Angeles, CA 90095-1595, USA
[b] MIIT Key Laboratory of Advanced Metallic and Intermetallic Materials Technology, Engineering Research Center of Materials Behavior and Design, Ministry of Education, Nanjing University of Science and Technology, Nanjing 210094, China
[c] Dept. of Materials Science and Engineering, National Yang Ming Chiao Tung University, Hsinchu 30010, Taiwan, ROC

HIGHLIGHTS

- A unique 2-step sidewall Cu_3Sn IMC formation around Cu-Sn micro-pillars is first revealed.
- The low nucleation barrier for sidewall Cu_3Sn is proved by density functional theory.
- A kinetic model is proposed to predict the mean lateral growth rate of the sidewall IMC.

GRAPHICAL ABSTRACT

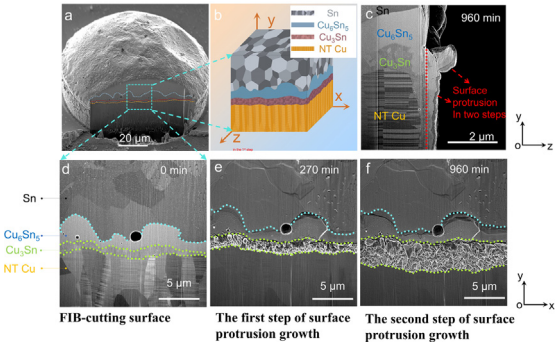

ARTICLE INFO

Article history:
Received 24 June 2022
Revised 25 September 2022
Accepted 26 October 2022
Available online 27 October 2022

Keywords:
Surface inter-diffusion
Intermetallic compounds (IMCs)
3D IC
Nucleation

ABSTRACT

With downward scaling of the micro-bumps in three-dimensional integrated circuits, surface inter-diffusion becomes dominant, changing the kinetic path of intermetallic compounds (IMC) formation and causing serious reliability issues. However, an in-depth understanding of the surface inter-diffusion process and the corresponding influence on the formation mechanism of IMC in a micro-bump remain unclear. We conducted annealing at 170 ℃, over 16 h for pillar type Sn/Cu micro-bumps and observed a unique 2-step sidewall Cu_3Sn IMC formation phenomenon on the FIB-cut clean surface of the micro-bumps. It is found the two-step sidewall IMC formation is dominated by the surface inter-diffusion of Sn and Cu atoms. Density functional theory calculations reveal that the activation energy barrier of nucleation for sidewall Cu_3Sn IMC is about 1/3 of that of sidewall Cu_6Sn_5 on corresponding interfacial IMC layers, making the formation of sidewall Cu_3Sn dominant. Moreover, we proposed a kinetic model that can predict the mean lateral growth rate of the sidewall IMC which may cause fatal short-circuit failure.

1. Introduction

Three-dimensional integrated circuits (3D ICs) have offered tremendous opportunities in semiconductor industry, as it meets the need for advanced electronic products for smaller form factor, multiple functions, faster rate of data transmission, cheaper cost, and superb reliability [1–5]. In 3D ICs, micro-pillar type bumps joining the through-Si vias (TSV) is the most distinctive structure for vertical stacking [6]. With downward scaling of micro-bumps, the density of input/output (I/O) interconnects increases, leading to higher bandwidth and lower power consumption for data transmission [3,7].

Yet, the size can greatly affect the microstructure and kinetic path [8,9]. Especially, surface diffusion becomes dominant with downward scaling of the micro-bumps, which results in new

* Corresponding authors at: Dept. of Materials Science and Engineering, Uni. of California, Los Angeles, CA 90095-1595, USA (K.N. Tu).
E-mail addresses: kntu@cityu.edu.hk (K.N. Tu), gchen@njust.edu.cn (G. Chen).
[1] These authors contributed equally to this work.

https://doi.org/10.1016/j.matdes.2022.111318
0264-1275/

reliability issues [10]. A new kind of sidewall intermetallic compounds (IMCs) are found to form and grow on the micro-bumps by surface diffusion [11–14]. The sidewall IMC was confirmed as Cu_3Sn, which forms during reflow (heating above the melting point of Sn) by molten Sn wetting the periphery of Cu pillar [9,12]. In the subsequent annealing, sidewall IMC continues to form on the uncovered Cu pillar by the surface diffusion of Sn [13,14]. Surface diffusion was considered to be the main driving force for sidewall IMC growth since the growth activation energy of them was calculated to be much smaller than that in previous studies where bulk or grain boundary diffusion dominates [13]. Sidewall IMC may lead to contacting between fine-pitch bumps causing short-circuit failure. Moreover, the overgrowth of the sidewall IMC is usually accompanied by consumption of Sn leading to serious voiding and necking in the tiny Sn solder [11,15] and possible formation of a porous interfacial Cu_3Sn layer in the micro-bump [16,17]. These changes severely degrade the mechanical properties of micro-bumps. It is thus of significance to have an in-depth understanding of the formation mechanism of sidewall IMC in micro-bumps and provide theoretical guidance to reduce reliability risk in 3D IC.

However, the mechanism of sidewall IMC formation and growth remains unclear. Previous studies ascribe the formation of sidewall Cu_3Sn IMC merely to the surface diffusion of Sn [10,13]. Whereas, it was revealed that abundant surface diffusion of Cu atoms during annealing of Cu/Sn micro pillar occurs [8,9]. Thus, instead of focusing on single species, the role of surface inter-diffusion of Cu and Sn atoms on the sidewall of Cu-Sn micro-bumps needs to be carefully examined. Considering the much lower diffusion activation energy for surface diffusion, inter-diffusion of Cu and Sn along the surface is energetically favored, driven by the concentration and chemical gradient (see Appendix 1). High-quality study of the surface inter-diffusion and its effects on formation mechanism of sidewall IMC requires diffusion marker, clean micro-bump surfaces, enough aging duration and proper time interval, which were not satisfied in previous reports. In the annealing of a Sn/Ni/Cu micro bump with a diameter of 20 μm, the periphery of the Cu pillar with a thickness of $\sim$ 3.5 μm was rapidly covered by newly formed sidewall Cu_3Sn which significantly hindered the surface diffusion of Cu atoms [13]. The oxidization contamination of the micro-bump surface also greatly impeded the surface diffusion process [14].

Herein, we utilize FIB-cutting to produce clean surfaces of Cu-Sn pillar type micro-bumps. Marker analysis, SEM, TEM and EDX characterization are performed to analyze the surface inter-diffusion of Cu and Sn atoms, the formation and growth of sidewall IMC on the micro-bumps. Density functional theory (DFT) calculations were conducted to elucidate the mechanisms at atomic scale. In addition, a kinetic model is proposed to explain the tendency of the sidewall Cu_3Sn IMC growth, which can be used to estimate the failure time for 3D IC, caused by short circuit due to the lateral growth of sidewall IMC.

2. Experimental

2.1. The fabrication of Cu/Sn wide free surface

The fabrication processes of Cu/Sn pillar-type samples were as follows: (a) A 100 nm SiO_2 layer was deposited on Si to prevent Cu-Si inter-diffusion. (b) A ⟨100⟩ oriented Cu layer was deposited on the silicon wafer to serve as a seed layer with a diameter of 100 μm. (c) The photoresist was spin coated and patterned by lithography. (d) The ⟨111⟩ oriented nano-twinned Cu (nt-Cu) was electroplated. (e) Sn solders were reflowed on Cu pillar at 260 ℃ for 2 min [19] (see the inset in Fig. 1a). The reflow will induce interfacial Cu_6Sn_5 formation of a thickness of about 5 to 10 μm as well as a thin interfacial layer of Cu_3Sn between the Cu and Sn (see Fig. 1b, c). After obtaining the 100 μm bumps, we use focused ion beam (FIB) to cut a 40 μm wide free surface on the bump (see Fig. 1b). Shown in Fig. 1b and c, we can clearly see the Cu/Sn bump has four layers which are Sn, Cu_6Sn_5, Cu_3Sn, and nt-Cu, before subsequent annealing to induce sidewall IMC formation. The FIB cutting was performed on a Zeiss Auriga cross-beam (FIB-SEM) workstation equipped with a Cobra gallium column and a Gemini electron column. To vividly demonstrate the potential threat due to the downsizing of micro-bump, several micro-pillars with diameters of 2 μm were also cut by FIB and annealed at 170 ℃ for 960 min (Fig. 1d-1f). It can be seen that surface protrusion with a thickness of 1.4 μm forms on the sidewall of 2 μm micro-pillars. Fine-pitch micro-bump usually has a distance approximately equal to its diameter from the adjacent micro-bump [6], this surface protrusion would cause contact with adjacent pillars and induce early-stage failure. The potential failure renders our following work on the mechanism of surface protrusion formation on a Cu/Sn free surface urgent.

2.2. Annealing treatment for Cu/Sn wide free surface

Once the Cu/Sn free surfaces are fabricated, the samples were put into a vacuum oven and annealed at 170 ℃ for 30, 60, 90, 150, 210, 270 and 960 min. The manifest pressure is 10^{-5} Pa. All the SEM micrographs were taken to record and observe the phenomena of sidewall IMC growth. The cross-sectional (y-z) plane (see Fig. 3a) is cut by FIB, to measure how much sidewall IMC was formed. The IMC is very soft, and it will be etched away even by ion beam observation. Consequently, we used magnetron sputtering technique to sputter a thin layer of tantalum (Ta) to protect the IMC from etching away.

2.3. Density functional theory calculations

To explain the mechanism of the unique formation of lateral Cu_3Sn IMC, the nucleation thermodynamics of sidewall Cu_3Sn and Cu_6Sn_5 on interfacial Cu-Sn IMC layers were analyzed based on the activation barrier energy of nucleation by DFT [20]. To obtain the activation barrier energy of nucleation, the calculation of formation enthalpy and surface energy is required. We employed the monoclinic η'-Cu_6Sn_5 (space group $C2/c$) and orthorhombic ε-Cu_3Sn (space group $Pmmn$) as starting configurations to calculate the formation enthalpy [21–23]. For the calculation of surface energies, 2×2 slabs with 7 layers were constructed to model various typical surfaces of Cu_6Sn_5 and Cu_3Sn. These surfaces include $Cu_3Sn(001)$, $Cu_3Sn(010)$, $Cu_3Sn(100)$, $Cu_3Sn(110)$, $Cu_3Sn(101)$ and $Cu_3Sn(111)$, $Cu_6Sn_5(001)$, $Cu_6Sn_5(010)$, $Cu_6Sn_5(100)$, $Cu_6Sn_5(110)$, $Cu_6Sn_5(101)$ and $Cu_6Sn_5(111)$ surfaces. For all slabs, the top and bottom three layers were relaxed while other layers were frozen. The calculations were performed with the generalized gradient approximation [24] for the exchange and correlation functional and the projected augmented wave approach [25] to represent the electron–ion interaction. Plane-wave cutoff energy of 400 eV was applied in all calculations. To aid convergence, the Fermi-level smearing approach of Methfessel and Paxton [26] was employed at a Gaussian width of 0.05 eV. Optimized atomic geometries were achieved when forces on all unconstrained atoms were smaller in magnitude than 0.01 eV/Å.

To verify the accuracy of our model, we first simulated the lattice parameters of Cu_6Sn_5 and Cu_3Sn. The lattice constants a, b and c of ε-Cu_3Sn are 5.571, 4.857, and 4.321 Å, respectively, with a difference within 2 % from the experimental results (a = 5.529 Å, b = 4.775 Å, and c = 4.323 Å) [21]. The lattice constants a, b, c, β of η'-Cu_6Sn_5 are 11.126, 7.367, 9.866 Å and 98.7° respectively, showing a deviation within 2 % from the experimental results (a = 11.022 Å, b = 7.282 Å, c = 9.827 Å and β = 98.84°) [27].

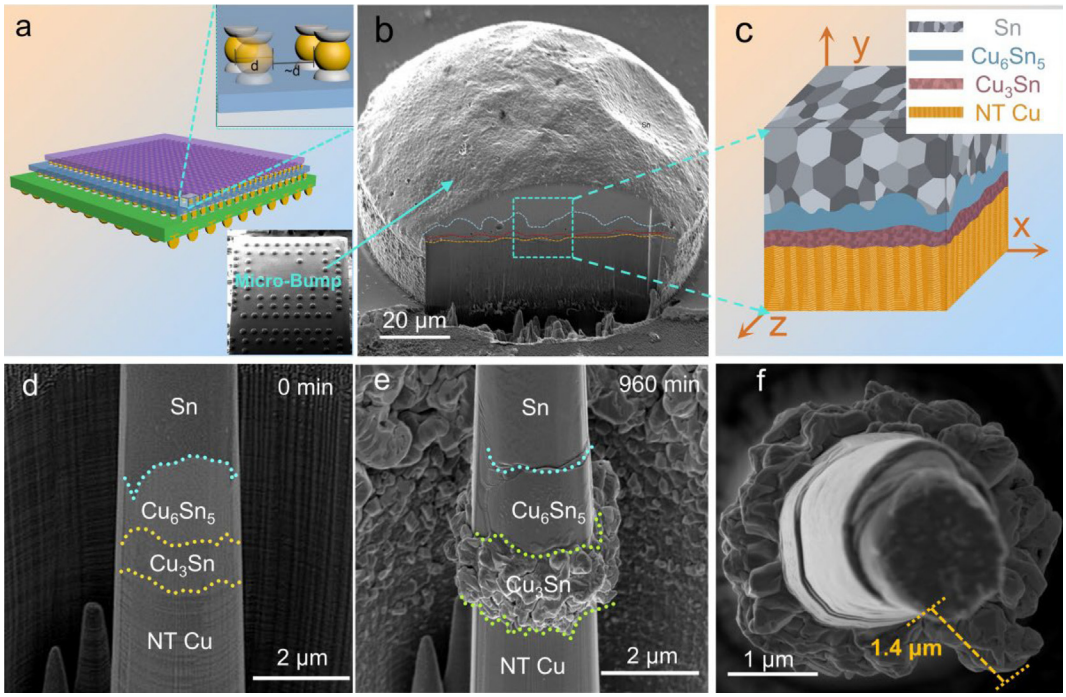

Fig. 1. (a) 3D model and (b) the SEM micrograph of a micro-bump showing the wide free surface cut by FIB. (c) Illustration of the square area in (b) revealing four layers of different phases distributed in a bump: Sn, Cu_6Sn_5, Cu_3Sn, and nt-Cu. (d)-(e) SEM images of surface protrusion in 2 μm diameter Sn/Cu pillar after annealing at 170 ℃ of 0 min and 960 min. (f) Top view of the 2 μm pillar which is annealed under 170 ℃ for 16 h, and the largest length of the sidewall IMC's lateral growth is 1.4 μm.

3. Results and analysis

3.1. A two-step formation of sidewall IMC

SEM cross-sectional micrograph of a Sn/Cu bump before annealing treatment, as depicted in Fig. 2a, shows a four-layer microstructure of Sn, Cu_6Sn_5, Cu_3Sn, and nt-Cu from top to the bottom. Fig. 2a-h show the change of the nt-Cu/Sn surface with annealing time at 170 ℃. From 0 to 270 min, it shows that surface protrusion starts to form on top of the interfacial Cu_3Sn surface and keeps growing thicker in the z direction, vertical to the x-y plane. With increasing aging time, the surface protrusion will grow on the Cu surface.

Fig. 3a shows the cross-sectional micrograph of the y-z plane, the red dash line represents the original surface of the free surface sample. According to TEM results, the surface protrusion was identified to be intermetallic compound of Cu_3Sn (see Fig. 3b). It shows that once the Sn atoms react with Cu substrate, IMCs form both in and on the surface of Cu layer.

Therefore, based on the SEM observation of the free surface sample annealed, a two-step sidewall IMC formation phenomenon could be identified. In the first step, the sidewall IMC forms much

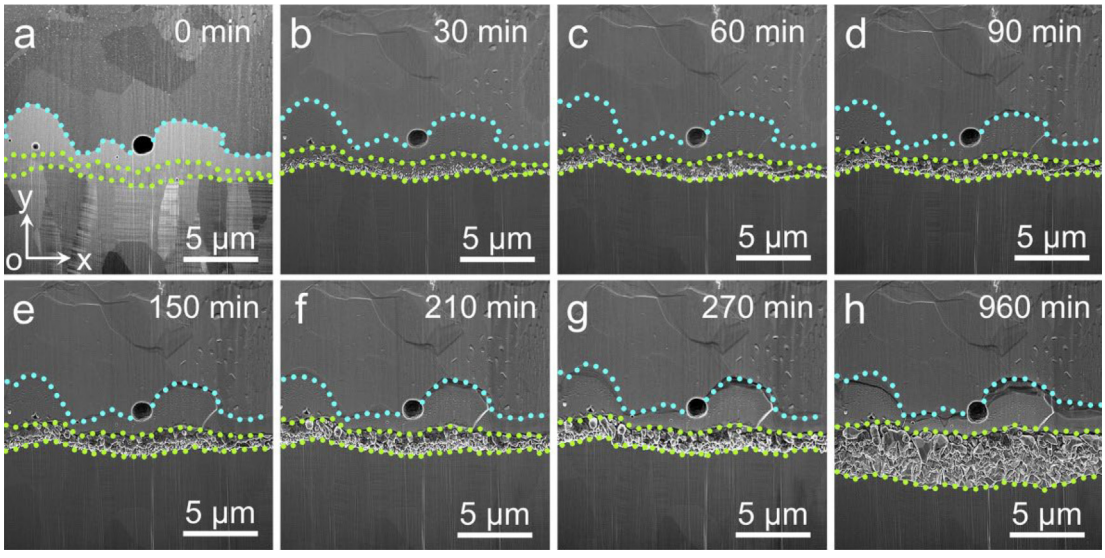

Fig. 2. (a) SEM micrograph of the Cu-Sn surface before heat treatment in x-y plane. (b)-(h) Semi-in-situ observations of Cu-Sn surface after annealing from 30 min to 960 min at 170 ℃. All SEM micrographs show a four-layer microstructure of Sn, Cu_6Sn_5, Cu_3Sn, and nt-Cu from top to the bottom. The dashed lines outline the interphases boundaries for better observation.

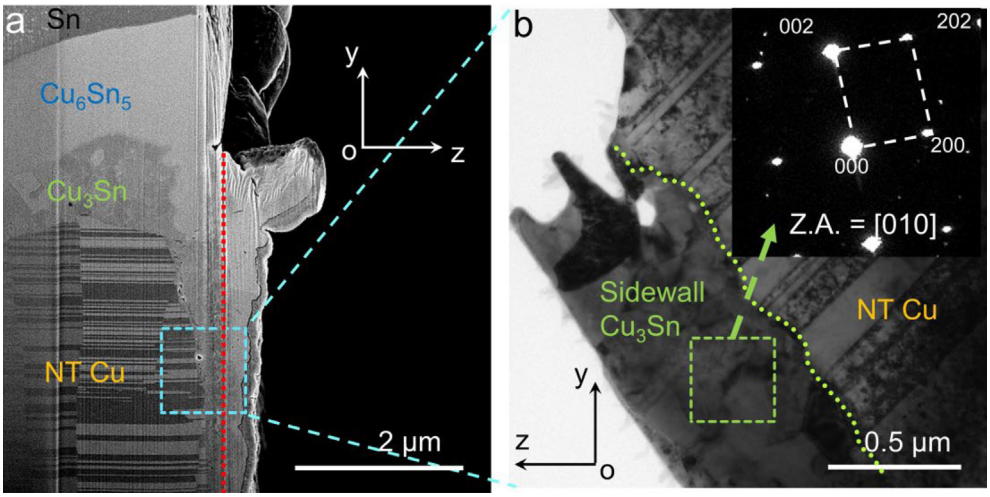

Fig. 3. (a) y-z plane SEM micrograph of the free surface sample annealed at 170℃ for 960 min, the red dash line represents the location of the original clean surface before annealing. (b) TEM micrograph showing the microstructure of the sidewall IMC formed and the inset is [0 1 0] selected area electron diffraction (SAED) patterns of Cu_3Sn. (For interpretation of the references to colour in this figure legend, the reader is referred to the web version of this article.)

faster on the surface of the interfacial Cu_3Sn layer than on that of any other layers. The sidewall IMC grows laterally in this step. In the second step, the sidewall IMC will form on the Cu surface. Furthermore, we found much more sidewall IMC has formed on the interfacial Cu_3Sn layer than on Cu_6Sn_5 layer (see Fig. 2b-h, and Fig. 3a) which will be discussed later.

3.2. EDX characterization of the concentration of Cu and Sn on Cu-Sn sample with free surface

To analyze the mechanism of two-step sidewall IMC formation, we first acquire the concentration variation of Cu and Sn elements on the cutting surfaces of Cu-Sn pillar bump annealed for 960 min at 170 ℃ using EDX. The EDX results of both x-y and y-z plane are tested (Fig. 4). The result on the x-y plane along the yellow line in Fig. 4a-4b shows that Sn concentration decreases continuously from the Sn side (Point A) to Cu side (Point B). On the Cu side, there is no trace of Sn where there is no newly formed Cu_3Sn IMC while excessive Cu is found on the Sn side. The result on the y-z plane along the red line in Fig. 4c-d shows that Cu concentration drops rapidly from the surface (Point C) to the inside of the Sn layer (Point D). It suggests Cu atoms move to the surface of Sn layer by surface diffusion and diffuse interstitially inward. The above results prove that Cu and Sn surface inter-diffusion takes place, and all the Sn atoms are consumed in forming sidewall Cu_3Sn on interfacial Cu_3Sn and nt-Cu surface (Fig. 3a). In addition, the Cu to Sn ratio of the surface protrusion on interfacial Cu_6Sn_5 and Cu_3Sn surfaces proves Cu_6Sn_5 and Cu_3Sn sidewall IMCs have formed over two interfacial IMC layers, respectively [13].

3.3. Marker analysis of the surface inter-diffusion of Cu and Sn atoms on the wide free surface

To elucidate the inter-diffusion of Cu and Sn atoms on the bump surface and the effects on sidewall IMC growth, marker analysis which is widely utilized to analyze the Kirkendall effect on the inter-diffusion phenomenon has been carried out in this work. According to Darken's theory, the marker tends to move against the faster diffusing atoms, which is in the same direction as the vacancy flux [28]. As shown in Fig. 5a-e, an intrusion spot on the Sn surface was selected as the immobile Marker I, and the indented void on the Cu_6Sn_5 surface as the mobile Marker II. In the first stage, the IMCs form only on the surface of interfacial Cu_3Sn and Marker II moves to the Cu side. In the second stage where IMCs form in the nt-Cu substrate, however, the marker moves to the Sn side in the opposite direction. This process is illustrated in Fig. 6. This is because the marker moves in the same direction as the net vacancy flux. As a result, the direction of vacancy flux has changed in the second step.

In the first step, the atom flux goes from Cu side to Sn side, including the bulk flux J_{Cu_B} of Cu and the surface flux J_{Cu_s} of Cu, while the atom flux from Sn side to Cu side only includes the bulk flux of Sn J_{Sn_B}. This is because the total surface flux of Sn J_{Sn_s} forms IMCs on the surface of interfacial Cu_3Sn layer and thus it does not reach the Cu side. Hence, the vacancy flux in the first step is $J_v = J_{Cu_B} + J_{Cu_s} - J_{Sn_B}$.

In the second step, part of J_{Sn_s} starts to diffuse into the nt-Cu substrate and results in an increase of the atom flux from Sn side to Cu side, namely, $J\prime_{Sn_s}$. Hence, the vacancy flux at the second stage is $J\prime_v = J_{Cu_B} + J_{Cu_s} - J_{Sn_B} - J\prime_{Sn_s}$. The value of the near-surface vacancy flux is changed with the extra $J\prime_{Sn_s}$, so that the movement direction of the Marker II is also changed. Conclusively, the experimental results of marker movement provide strong evidence for the two-step sidewall IMC formation in the Cu-Sn pillar-type micro-bumps.

3.4. Theoretical calculations of the activation energy barriers of nucleation for sidewall Cu_3Sn and Cu_6Sn_5 IMCs

The formation of sidewall Cu_3Sn and Cu_6Sn_5 is affected by both inter-diffusion and nucleation as depicted in Fig. 7. According to marker analysis and concentration variation results (see Fig. 4, Fig. 5), we know sufficient inter-diffusion of Cu and Sn takes place on both interfacial Cu_3Sn and Cu_6Sn_5 layer surfaces. Therefore, sidewall Cu-Sn IMCs are supposed to form on both IMC layers according to the phase diagram of Cu-Sn binary alloy [29]. However, sidewall Cu_3Sn grows much faster than sidewall Cu_6Sn_5 (see Fig. 2b-g) which implies nucleation is more likely to play the major role. Herein, we conducted DFT calculations to estimate and compare the activation energy barriers of nucleation for sidewall Cu_3Sn IMC and sidewall Cu_6Sn_5 IMC.

The activation energy barrier ΔG^* for heterogeneous nucleation [30] can be presented in terms of the wetting angle (θ) and the cap radius (r) as.

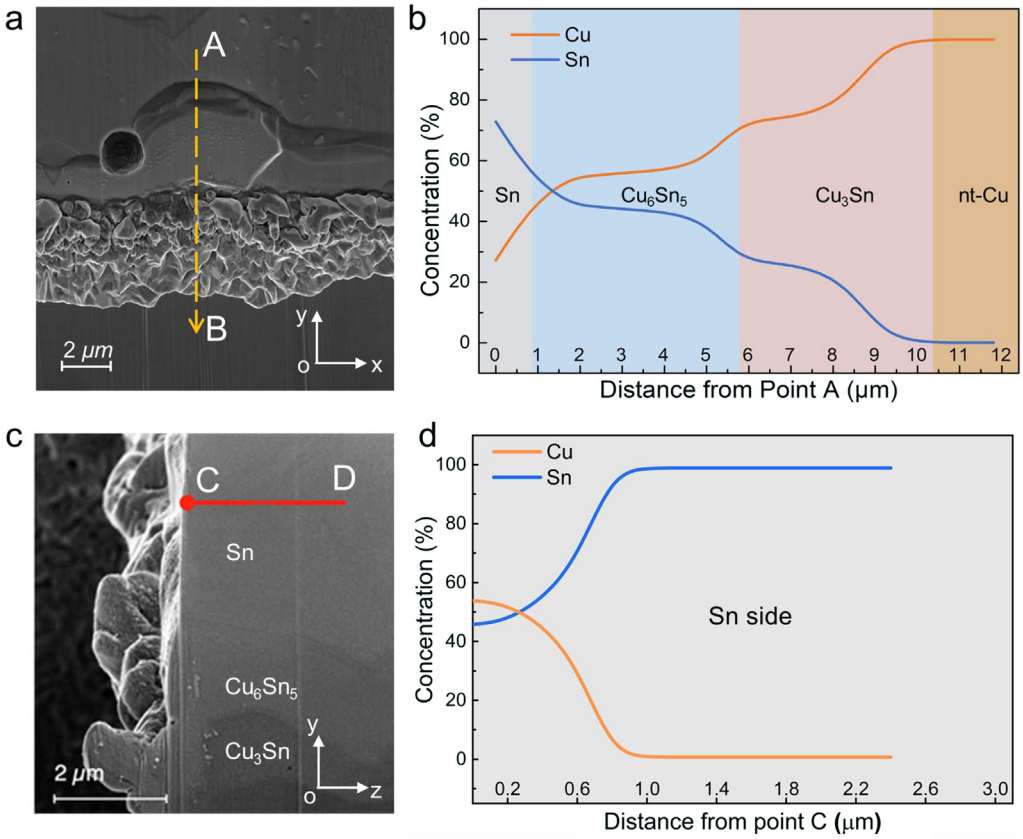

Fig. 4. (a) SEM micrograph of Cu-Sn sample with wide free surface after annealing for 960 min at 170 ℃. The observation direction is from z axis. (b) Concentration variation of Cu and Sn on the cutting surface of Cu-Sn bump sample by EDX along the line from point A to B. (c) The y-z plane SEM micrograph of Cu-Sn sample with wide free surface. (d) Concentration variation of Cu and Sn on the y-z plane surface of Cu-Sn bump sample along the line from point C to D.

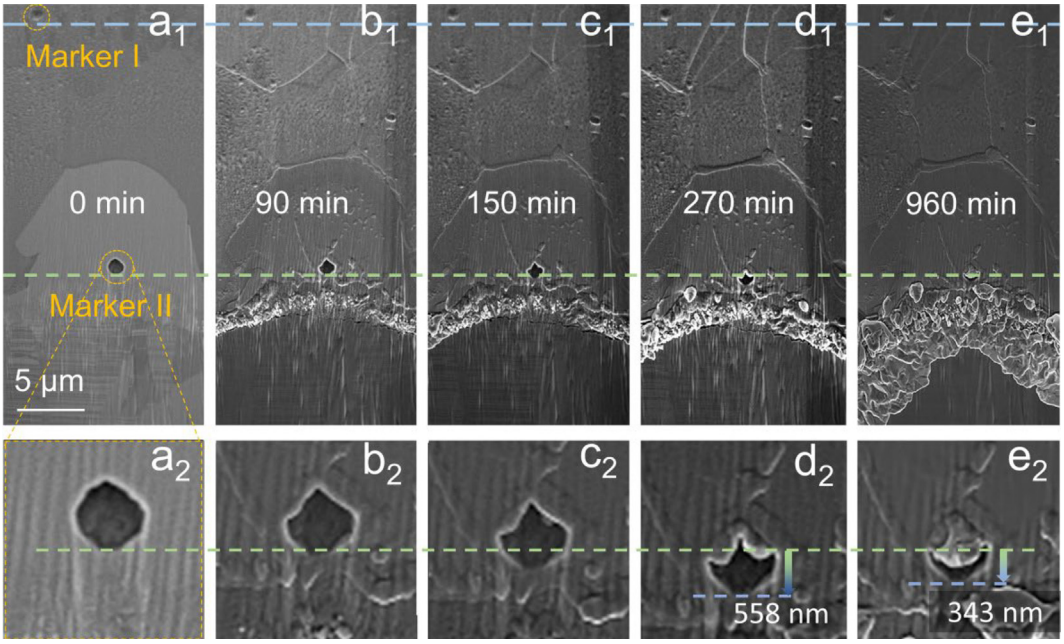

Fig. 5. (a1)-(e1) Semi-in-situ marker motion observation after annealing from 0 to 960 min at 170 ℃. Marker I is an intrusion on the Sn surface, and Marker II is a surface void lying in Cu_6Sn_5. The blue dash line represents the position of Marker I, and the green dash line stands for the original position of Marker II before annealing. (a2)-(e2) The enlarged images of Marker II. The green dash line represents the original position of Marker II at 0 min, and the blue dash line in d_2 and e_2 represents the position at the corresponding time. (For interpretation of the references to colour in this figure legend, the reader is referred to the web version of this article.)

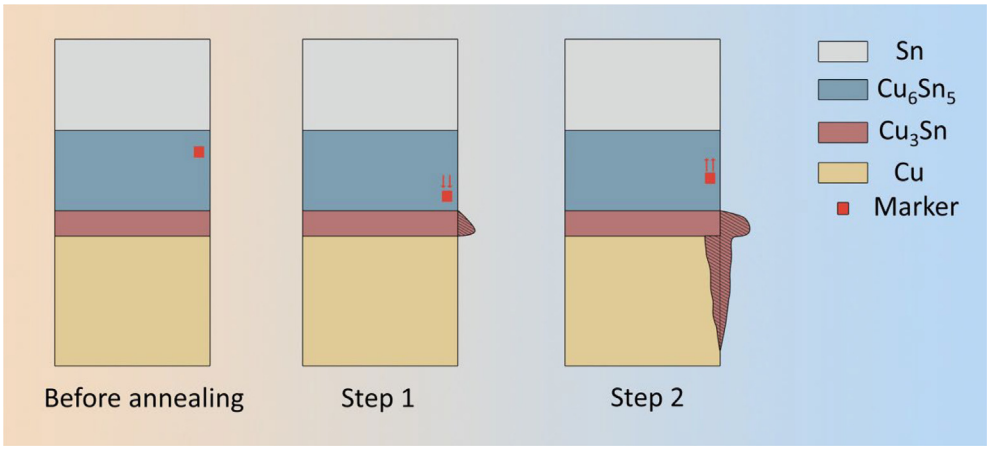

Fig. 6. Illustration of the process of the two-step sidewall IMC formation.

$$\Delta G^{*} = \frac{16\pi\gamma_{ms}^{3}}{3\Delta G_{v}^{2}} S(\theta) \tag{1}$$

$$S(\theta) = (2+\theta)(1-\cos(\theta))^{2}/4 \tag{2}$$

$$\gamma_{mv} = \gamma_{ms} + \gamma_{sv}\cos(\theta) \tag{3}$$

where the wetting angle θ is given by the balance among the interfacial tensions γ_{ms}, γ_{sv} and γ_{mv} [31]. γ_{ms}, γ_{sv} and γ_{mv} are respectively the interfacial energies of the sidewall Cu-Sn IMC/interfacial Cu-Sn IMC layer surface, the sidewall Cu-Sn IMC/vapor and interfacial Cu-Sn IMC layer surface/vapor interface. ΔG_v is the volume free energy change when forming a solid embryo on the surface.

To obtain the accurate activation energy barrier of nucleation, we need the value of γ_{sv}, ΔG_v and the wetting angle θ of the newly formed Cu-Sn IMC on the interfacial Cu-Sn IMC surface (Eq. (1)). Since no experimental data on Cu_3Sn and Cu_6Sn_5 surface energy are available to our knowledge, the surface energies of Cu_3Sn and Cu_6Sn_5 are obtained from DFT calculations according to Eq. (A4) in the Appendix [32]. The surface energies of various typical surfaces of Cu_3Sn and Cu_6Sn_5 are calculated employing slabs shown in Fig. 8b and 8c. The obtained results are summarized in Table A1 in the Appendix. The surface energy varies from 0.76 to 0.95 J/m^2 with the orientations. Hence, we take the average value of 0.86 J/m^2 and 0.83 J/m^2 as the surface energies of Cu_3Sn and Cu_6Sn_5 respectively. The wetting angles of sidewall Cu_3Sn and Cu_6Sn_5 on the interfacial IMC layers are supposed to be very small since the newly formed sidewall IMC prefers to have an identical orientation with the IMC layer to minimize the lattice misfit energy and interface energy [33–35]. Due to the difficulty in obtaining the value experimentally, we simply assume the wetting angles of both sidewall Cu_3Sn and Cu_6Sn_5 on the IMC surface to be the same with a small value.

The ΔG_v can be calculated as the formation enthalpy if the entropy term in the free energy is ignored as in the present experiment at low temperature [36]. The formation enthalpy is given as [37],

$$\Delta E(Cu_mSn_n) = \frac{1}{m+n} E_{Cu_mSn_n} - \left[\frac{m}{m+n} E_{Cu} + \frac{n}{m+n} E_{Sn}\right] \tag{4}$$

where $E_{Cu_mSn_n}$ is the total energy of bulk Cu_mSn_n. We employed the monoclinic η'-Cu_6Sn_5 and orthorhombic ε-Cu_3Sn (Fig. 8a) as starting configurations to calculate the formation enthalpy. E_{Cu} is the total energy per atom with the face-centered cubic structure and E_{Sn} is the total energy per atom of Sn with the *A5*-tetragonal structure. The formation enthalpy of Cu_3Sn and Cu_6Sn_5 based on Eq. (4) are listed in Table 1 along with previous theoretical and experimental results for comparison.

As shown in Table 1, the calculated formation enthalpy of Cu_6Sn_5 and Cu_3Sn are −4.75 kJ/mol·atom and −5.46 kJ/mol·atom, respectively. The formation enthalpy from our work exhibits a small deviation from other DFT calculations about 0.5–0.8 kJ/mol·atom except the one from Gao's work [38]. The values are different from those obtained by experiments or Calphad methods [36] by about 2.5 kJ/mol·atom. However, the formation enthalpy of Cu_3Sn in our work is about 1.15 times that of Cu_6Sn_5 which shows good consistency with previous theoretical and experimental results [36,41,42]. Substituting the surface energy, wetting angle and formation enthalpy into Eq. (1), the activation energy barrier of nucleation for Cu_3Sn and Cu_6Sn_5 are calculated as 1.829e-19 kJ/m^3 and 5.259e-19 kJ/m^3 and respectively.

The activation energy barrier of nucleation for sidewall Cu_3Sn on interfacial Cu_3Sn surface is about 1/3 of that for sidewall Cu_6Sn_5 on interfacial Cu_6Sn_5 surface, resulting in a larger nucleation rate of sidewall Cu_3Sn. The interfacial Cu_3Sn layer serves as energetically favorable nucleation sites for sidewall Cu_3Sn which accounts for the prominent lateral growth of sidewall Cu_3Sn IMC in the first step (Fig. 3a, Fig. 6). The lateral growth in the first step due to its large thickness poses the biggest threat of contacting failure of bumps. It is noteworthy that if Sn fluxes reaching the surface of the sidewall Cu_3Sn grown in the first step could not be completely spent, the concentration gradient of Sn from the surface of sidewall Cu_3Sn to the adjacent Cu surface increases. Therefore, excessive Sn flux from the surface of sidewall Cu_3Sn, driven by the increased concentration gradient, transports to Cu surface and forms Cu_3Sn in the second step.

The prevailing nucleation of sidewall Cu_3Sn over Cu_6Sn_5 in a surface diffusion dominated system is opposite from that in a bulk diffusion dominated system such as ball-grid-array (BGA) or controlled-collapse-chip- connection (C4) micro joints [6] in the 3D IC industry, where Cu_6Sn_5 nucleates first before Cu_3Sn [43]. This difference was thought to be caused by the much larger interface energy of the Cu_3Sn/Cu interface in the bulk diffusion dominated system than that of the Cu_6Sn_5/Cu interfaces [34,44] despite the greater formation enthalpy of Cu_3Sn.

3.5. A kinetic model of two-step formation of sidewall IMC

A kinetic model is presented below to reveal the IMC formation process and to forecast the lateral growth rate of the sidewall IMC. The latter is technically important because it may cause a short circuit by contacting neighboring pillar bumps. We approximate that

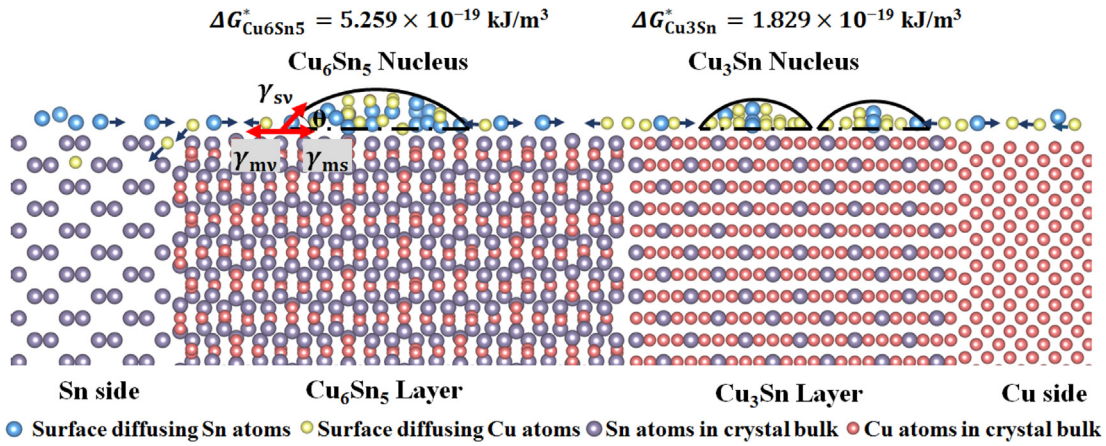

Fig. 7. Illustration of the formation and growth of sidewall Cu_3Sn and Cu_6Sn_5 IMC influenced by nucleation and adatoms diffusion. The energy barrier of nucleation of sidewall Cu_6Sn_5 ($\Delta G^*_{Cu_6Sn_5}$) and Cu_3Sn ($\Delta G^*_{Cu_3Sn}$) IMC calculated by DFT are written as well.

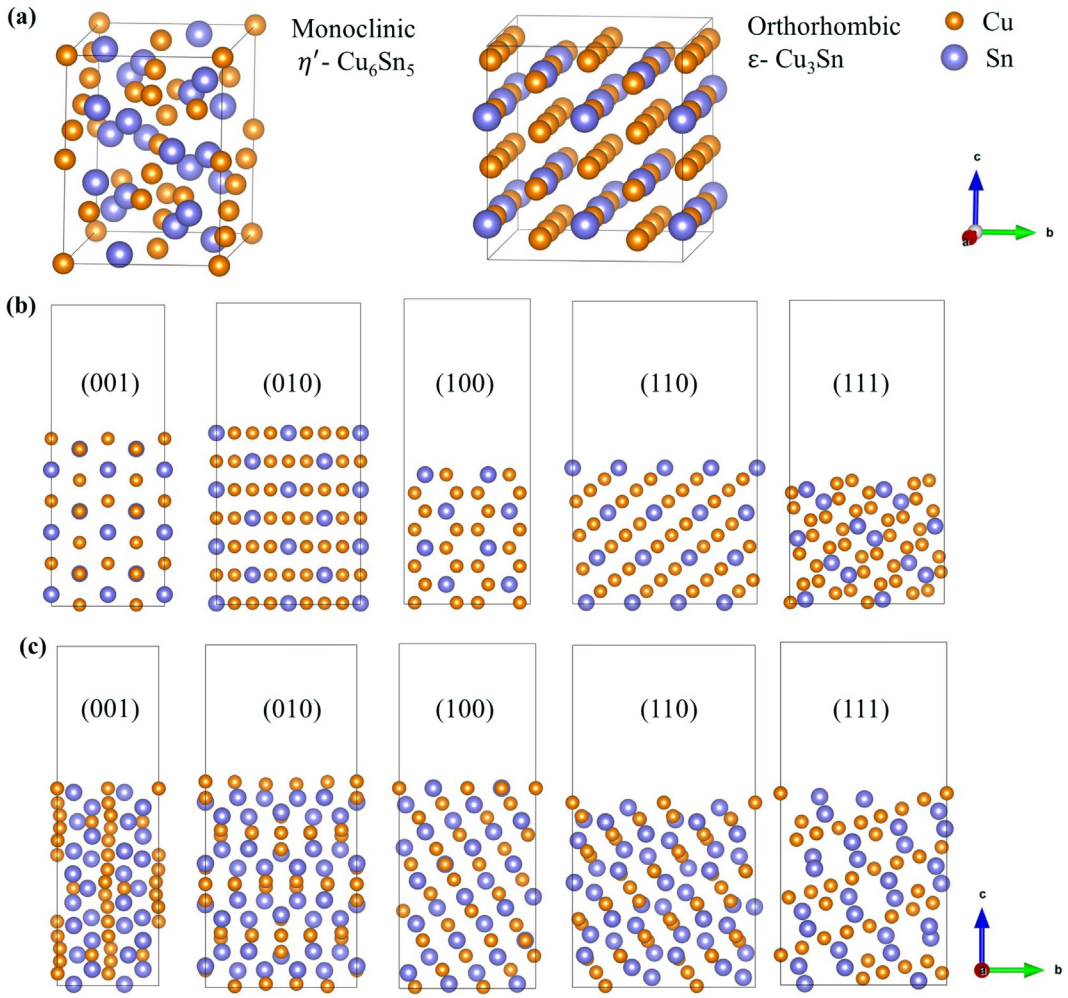

Fig. 8. (a) Crystal structures of Monoclinic η'-Cu_6Sn_5 and Orthorhombic ε-Cu_3Sn phases respectively to calculate the formation enthalpy. (b) Cu_3Sn surface models with five typical orientations. (c) Structure of Cu_6Sn_5 surface models with five typical orientations.

the sidewall IMC has a roof shape with length l and width W, and grows on a Cu_3Sn layer with a thickness H, which can be regarded as a constant since the thickness of the bulk Cu_3Sn layer almost does not change during the annealing process at 170 ℃. Since the Cu_3Sn is next to the Cu, there are sufficient Cu atoms that will immediately react with those Sn atoms that diffuse from Sn side to form Cu_3Sn. As a result, the growth rate is controlled by the surface flux J_{Sn_5} of Sn.

In Fig. 9b, the orange dots represent the experimental lateral lengths of the sidewall IMC, annealed under 170 ℃, from 8 groups

Table 1
A comparison of the formation enthalpy of Cu_3Sn and Cu_6Sn_5 obtained by various methods: ab initio calculations (at 0 K), experiment, and CALPHAD (at 298.15 K) basing on the reference states of *fcc*-Cu and *bct*-Sn. E_{Cu6Sn5} and E_{Cu3Sn} denote the formation enthalpy of Cu_6Sn_5 and Cu_3Sn.

E_{Cu6Sn5} (kJ/mol·atom)	E_{Cu3Sn} (kJ/mol·atom)	Method
−4.75	−5.46	Our work,GGA
−4.02	—	DFT,LDA [37]
−5.23	—	DFT,GGA [38]
−10.438	−11.789	DFT,GGA [39]
−6.2	−5.4	EHF model [40]
−7.13	−8.194	Calphad Method [36]
−5.8	−7.7	Experiment [41]
−6.1	−8.2	Experiment [42]

of samples (shown in Fig. 9a). The length of IMC almost increases linearly within the time from 0 to 4 h, thus $dl = kdt$, where k is a constant. If we assume the IMC is a roof shape, the volume gained, dV in time dt is,

$$dV = J_{Sn_s}\bar{A}\Omega dt \tag{5}$$

$$dV = \frac{1}{2}(W + dW)H(l + dl) - \frac{1}{2}WHl \tag{6}$$

If we assume that the sidewall IMC remains roof shape and W increases proportionally with l, thus $dW = adl$, where a is the proportional constant to describe the width change as the length grows. Equating (5) and (6), we obtain.

$$J_{Sn_s} = \frac{(WH + aHl)}{2\bar{A}\Omega}\cdot\frac{dl}{dt} \tag{7}$$

which is an expression of surface flux of Sn, coming from Sn side to Cu side, where $\bar{A}$ is the mean diffuse area, $\bar{A} = \frac{Wd_{Sn}}{2}$, d_{Sn} is the thickness of single atomic layer of Sn, d_{Sn} = 5 × 10^{-8} cm, and Ω is the molar volume of Cu_3Sn, Ω= 35 cm^3/mol.

As shown in Fig. 9b, after 4 h of annealing, the mean length of the sidewall IMC is $l = 539nm$. The length of IMC increased almost linearly in the initial 4 h, $\frac{dl}{dt} = \frac{\Delta l}{\Delta t} = 3.47 \times 10^{-9}$ cm/s. When t = 0, l = 0, Eq. (7) becomes.

$$J_{Sn_s} = \frac{H}{\Omega d_{Sn}}\cdot\frac{dl}{dt} = 4.28 \times 10^{-7} mol/s \cdot cm^2 \tag{8}$$

Besides J_{Sn_s}, the growth of the IMC is also controlled by the flux, J_{roof}, which goes up the top of the roof from the surface boundary of Cu_6Sn_5 and Cu_3Sn as.

$$J_{roof} = -D_{Sn}\frac{\partial C}{\partial x} = -D_{Sn}\frac{\Delta C}{l} \tag{9}$$

According to the EDX results, when $t = 0$, the concentration difference between the Cu_6Sn_5/Cu_3Sn interface C_{bot} and the top of the roof C_{top} is.

$$\Delta C = C_{top} - C_{bot} = -0.004056\,\mathrm{mol/cm^3} \tag{10}$$

By acquiring the concertation difference, we obtain the value of,

$$J_{roof} = \frac{2.79 \times 10^{-11}}{l}\,\mathrm{mol/s\cdot cm} \tag{11}$$

If we assume the concentration difference between the top and the bottom of the roof stays constant, the concertation gradient decreases as the IMC roof grows higher.

When $J_{Sn_s} < J_{roof}$, all Sn atoms in flux are spent for Cu_3Sn roof growth. When $J_{Sn_s} > J_{roof}$, the extra Sn atoms will grow Cu_3Sn on Cu. Therefore, when the second step starts:

$$J_{Sn_s} = J_{roof} \tag{12}$$

Substituting Eq. (8) and (9) into Eq. (12):

$$4.28 \times 10^{-7}\,\mathrm{mol/s\cdot cm^2} = \frac{2.79 \times 10^{-11}}{l_{critical}}\,\mathrm{mol/s\cdot cm} \tag{13}$$

Thus, when the second step starts, the critical length $l_{critical}$ = 653 nm.

Meanwhile, when the extra flux $J\prime_{Sns}$ flows through IMC, the concentration at the top of the roof C_{top} will increase, which will further decrease J_{roof}. To simplify the model, we assume that the effect of excess flow rate on the concentration increase is linear, thus:

$$J\prime_{Sn_s} = J_{Sn_s} - J_{roof} \tag{14}$$

$$C_{top} = C_{top}(t = 0) + \eta J\prime_{Sns} \tag{15}$$

Substituting Eq. (16) into Eq. (11), when $l < l_{critical}$:

$$\Delta C = -0.004056\,\mathrm{mol/cm^3} + \eta J\prime_{Sns} \tag{16}$$

In the first step of sidewall IMC formation, the Sn flux follows the linear growth in the initial 4 h and also, we pointed out that when IMC length reaches $l_{critical}$, the top of the roof will grow slower than the bottom part. Hence, to describe the following non-linear growth in the second step, we need to calculate the flux of both the top part and the bottom part of the sidewall IMC and use the mean flux J_{mean} instead of initial flux J_{Sn_s} to study the change of V, and J_{roof} instead of J_{Sn_s} to study the change of l.

According to the formula of $\frac{dl}{dt}$, we can choose a small increment of Δl, herein 5 × 10^{-6} cm, and calculate W, H, h, J_{roof} and $\frac{dl}{dt}$ at each step of Δl with iteration from initial value $H = 1.5 \times 10^{-4}$ cm and $W = 5 \times 10^{-5}$ cm. Based on l-$\frac{dl}{dt}$ relationship, we can finally obtain numerically simulated t-l curve.

The growth rate equation is deduced as follows.

$$\frac{dl}{dt} = \begin{cases} \frac{J_{Sn_s}\Omega d_{Sn}}{HW + aHl}, l \le l_{critical} \\ \frac{J_{roof}W\Omega d_{Sn}}{HW + aHl}, l > l_{critical} \end{cases} \tag{17}$$

when a ranges from 0.02 to 0.05, and η ranges from 2000 to 3500, the calculated curve fits the best with the experimental results. And Fig. 9b shows the comparison between this modeling equation and experimental results.

4. Conclusion

We discovered a novel two-step formation of the sidewall Cu_3Sn IMC on the four-layered ($Sn/Cu_6Sn_5/Cu_3Sn/Cu$) clean surface of a micro-pillar. In the first step, the sidewall Cu_3Sn IMC forms much faster on the surface of interfacial Cu_3Sn layer than on any other layers. In the second step, the sidewall IMC will form on the Cu layer surface. The two-step sidewall IMC formation is dominated by the surface inter-diffusion of Sn and Cu atoms. Verified by marker motion, change of vacancy flux direction explains the starting point of the second step. Through DFT calculations, we reveal that the lower activation energy barrier of nucleation for sidewall Cu_3Sn contributes to its prevailing nucleation over sidewall Cu_6Sn_5. Moreover, we proposed a kinetic model that can estimate and predict the mean lateral growth rate of the sidewall IMC. The model is of practical value as short-circuit can be caused by the contacting of adjacent micro-bumps. Our work helps expose the surface inter-diffusion process and sidewall IMC formation mechanism in the miniaturized micro-bump, providing theoretical guidance to reduce the reliability risk in 3D ICs.

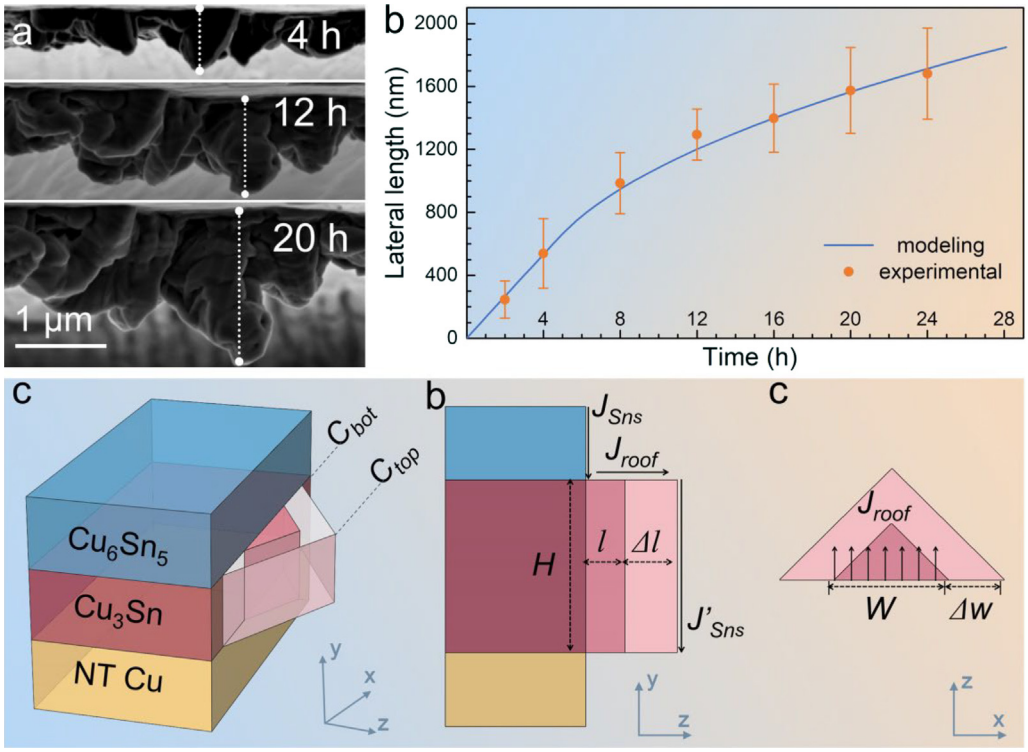

Fig. 9. (a) Experimental observation of the sidewall IMC growth. The observation direction is from y axis. (b) Experimental measurement results and theoretical calculation curve from kinetic model of the lateral growth of sidewall IMC under 170 °C. The orange dots represent the mean length measured from 8 groups of samples. The blue curve represents the calculation result based on our kinetic model. (c)-(e) Kinetic model for the lateral growth of sidewall IMC. (For interpretation of the references to colour in this figure legend, the reader is referred to the web version of this article.)

Data availability

The data that support the findings of this study are available from the corresponding authors upon reasonable request.

Data availability

Data will be made available on request.

Declaration of Competing Interest

The authors declare that they have no known competing financial interests or personal relationships that could have appeared to influence the work reported in this paper.

Acknowledgements

This study was supported by Ministry of Science and Technology, Taiwan (grant No. MOST 109-2634-F-009-028) and the Center for Emergent Functional Matter Science at National Chiao Tung University from The Featured Areas Research Center Program within the framework of the Higher Education Sprout Project by the Ministry of Education (MOE) in Taiwan.

Appendix

1. The surface inter-diffusion

Surface inter-diffusion refers to the atom-transport process where two different species of adatoms and atom clusters diffuse

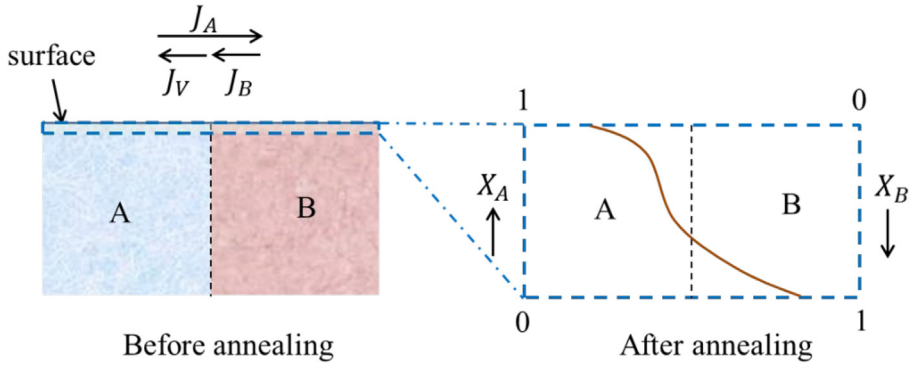

Fig. A1. Surface inter-diffusion of A and B, and concentration profile (red line) after surface inter-diffusion. X_A and X_B refer to the concentration of A and B respectively.

Table A1
The surface energies of various Cu_3Sn and Cu_6Sn_5 surfaces by ab initio calculation.

Cu_3Sn surfaces	surface energy(J/m^2)	Cu_6Sn_5 surfaces	surface energy(J/m^2)
(001)	0.76	(101)	0.79
(010)	0.79	(001)	0.78
(011)	0.91	(010)	0.93
(100)	0.87	(100)	0.85
(110)	0.92	(110)	0.85
(111)	0.94	(111)	0.78
average value	0.86	average value	0.83

mutually towards each other along the surface, driven by concentration and chemical potential gradients.

In details, the mathematical definition could be explained below. When the diffusion couple of pure A and B are annealed (Fig. A1), the surface inter-diffusion of A and B along the surface are greatly promoted compared with bulk diffusion within the bulk due to the much lower activation energy. As a result, the concentration profile near the surface is changed. Due to unequal diffusion rates and flux of A and B ($J_A > J_B$), there is a net flux of vacancies near the surface towards the faster diffusion specie A. The J_A, J_B and net flux of vacancies could be given as below.

$$J_A = -D_{SA}\frac{\partial C_A}{\partial x} \tag{A1}$$

$$J_B = -D_{SB}\frac{\partial C_B}{\partial x} \tag{A2}$$

$$J_v = -J_A - J_B \tag{A3}$$

where D_{SA} and D_{SB} are the surface diffusion coefficients of A and B species respectively.

2. Surface energy of various Cu_3Sn and Cu_6Sn_5 surfaces

The surface energy (Table A1) for each surface per unit area were calculated using the following equation,where E_{Slab} is the total energy of the slab, $N_{Cu_mSn_n}$ is the number of Cu_mSn_n units inside the slab, $E_{Cu_mSn_n-bulk}$ is the total energy of the corresponding bulk structure per Cu_mSn_n unit and finally A is the surface area of the slab.

References

[1] K.-N.-N. Chen, K.-N.-N. Tu, MRS Bull. 40 (2015) 219–222.
[2] K.N.N. Tu, Microelectron. Reliab. 51 (2011) 517–523.
[3] S. Annuar, R. Mahmoodian, M. Hamdi, K.N. Tu, Sci. Technol. Adv. Mater. 18 (2017) 693–703.
[4] C. Erdmann, D. Lowney, A. Lynam, A. Keady, J. McGrath, E. Cullen, D. Breathnach, D. Keane, P. Lynch, M. De La Torre, R. De La Torre, P. Lim, A. Collins, B. Farley, L. Madden, IEEE J. Solid-State Circuits 50 (2015) 258–269.
[5] A.K. Ramanathan, S.S. Rangachar, J.-M. Hung, C.-Y. Lee, C.-X. Xue, S.-P. Huang, F.-K. Hsueh, C.-H. Shen, J.-M. Shieh, W.-K. Yeh, M.-S. Ho, H.T. Govindarajan, J. Sampson, M.-F. Chang, V. Narayanan, in: 2020 IEEE Int. Electron Devices Meet., IEEE, 2020, pp. 28.5.1-28.5.4.
[6] C. Chen, D. Yu, K.-N. Chen, MRS Bull. 40 (2015) 257–263.
[7] R.S. Patti, Proc. IEEE 94 (2006) 1214–1224.
[8] Y. Liu, Y.-C.-C. Chu, K.N.N. Tu, Acta Mater. 117 (2016) 146–152.
[9] Y. Liu, X. Shi, H. Ren, J. Cai, X. Zhao, C. Tan, K.N. Tu, Mater. Lett. 284 (2021) 129036.
[10] C. Yang, S. Ren, X. Zhang, A. Hu, M. Li, L. Gao, H. Ling, T. Hang, Mater. Charact. 159 (2020) 110030.
[11] Y.C. Liang, C. Chen, K.N. Tu, ECS Solid State Lett. 1 (2012) P60–P62.
[12] D. Wang, H. Ling, M. Sun, X. Miao, A. Hu, M. Li, F. Dai, W. Zhang, L. Cao, J. Mater. Sci. Mater. Electron. 29 (2018) 1861–1867.
[13] S. Ren, M. Sun, Z. Jin, Y. Guo, H. Ling, A. Min Hu, M. Li, Electron. Mater. Lett. 15 (2019) 562–571.
[14] C. Yang, X. Zhang, M. Dong, A. Hu, M. Li, L. Gao, H. Ling, T. Hang, Mater. Chem. Phys. 256 (2020) 123663.
[15] Y.-W. Chang, C. Hu, H.-Y. Peng, Y.-C. Liang, C. Chen, T. Chang, C.-J. Zhan, J.-Y. Juang, Sci. Rep. 8 (2018) 5935.
[16] D.T. Chu, Y.-C. Chu, J.-A. Lin, Y.-T. Chen, C.-C. Wang, Y.-F. Song, C.-C. Chiang, C. Chen, K.N. Tu, Microelectron. Reliab. 79 (2017) 32–37.
[17] Y.W. Wang, Mater. Chem. Phys. 275 (2022) 125307.
[19] H.-Y. Hsiao, C.-M. Liu, H.-W. Lin, T.-C. Liu, C.-L. Lu, Y.-S. Huang, C. Chen, K.N. Tu, Science (80-.) 336 (2012) 1007–1010.
[20] G. Kresse, J. Furthmüller, Phys. Rev. B 54 (1996) 11169–11186.
[21] Y. Watanabe, Y. Fujinaga, H. Iwasaki, Acta Crystallogr. Sect. B Struct. Sci. 39 (1983) 306–311.
[22] R. An, C. Wang, Y. Tian, H. Wu, J. Electron. Mater. 37 (2008) 477–482.
[23] N.T.S. Lee, V.B.C. Tan, K.M. Lim, Appl. Phys. Lett. 88 (2006) 1–3.
[24] J.P. Perdew, K. Burke, M. Ernzerhof, Phys. Rev. Lett. 77 (1996) 3865–3868.
[25] P.E. Blöchl, Phys. Rev. B 50 (1994) 17953–17979.
[26] M. Methfessel, A.T. Paxton, Phys. Rev. B 40 (1989) 3616–3621.
[27] A.-K. Larsson, L. Stenberg, S. Lidin, Acta Crystallogr. Sect. B Struct. Sci. 50 (1994) 636–643.
[28] H.J. Fan, U. Gösele, M. Zacharias, Small 3 (2007) 1660–1671.
[29] K. Nogita, C.M. Gourlay, T. Nishimura, Jom 61 (2009) 45–51.
[30] D.A. Porter, K.E. Easterling, Phase Transformations in Metals and Alloys, 2nd ed., Springer, US, Boston, MA, 1992.
[31] H. Wang, F. Gao, X. Ma, Y. Qian, Scr. Mater. 55 (2006) 823–826.
[32] E. German, R. Faccio, A.W. Mombrú, Appl. Surf. Sci. 428 (2018) 118–123.
[33] K.K. Wang, D. Gan, K.C. Hsieh, Thin Solid Films 562 (2014) 398–404.
[34] Z. Zhang, H. Cao, M. Li, Y. Yu, H. Yang, S. Yang, Mater. Des. 94 (2016) 280–285.
[35] J.H. Ke, Y. Gao, C.R. Kao, Y. Wang, Acta Mater. 113 (2016) 245–258.
[36] J.H. Shim, C.S. Oh, B.J. Lee, D.N. Lee, Zeitschrift Fuer Met. Res. Adv. Tech. 87 (1996) 205–212.
[37] G. Ghosh, M. Asta, J. Mater. Res. 20 (2005) 3102–3117.
[38] F. Gao, J. Qu, T. Takemoto, J. Electron. Mater. 39 (2010) 426–432.
[39] Y. Yang, H. Lu, C. Yu, J. Chen, in: 2009 Int. Conf. Electron. Packag. Technol. High Density Packag. ICEPT-HDP 2009 (2009) 384–387.
[40] R. Pretorius, T.K. Marais, C.C. Theron, Mater. Sci. Rep. 10 (1993) 1–83.
[41] H.C. Cowen, Chem. Eng. Sci. 6 (1957) 234.
[42] H. Flandorfer, U. Saeed, C. Luef, A. Sabbar, H. Ipser, Thermochim. Acta 459 (2007) 34–39.
[43] J.F. Li, P.A. Agyakwa, C.M. Johnson, Acta Mater. 59 (2011) 1198–1211.
[44] J.O. Suh, K.N. Tu, N. Tamura, J. Appl. Phys. 102 (2007).